

Size effects and strength fluctuation in nanoscale plasticity

Wei Wang^a, Yuan Zhong^b, K. Lu^a, Lei Lu^a, David L. McDowell^{b,c}, Ting Zhu^{b,*}

^aShenyang National Laboratory for Materials Science, Institute of Metal Research, Chinese Academy of Sciences, Shenyang 110016, China

^bWoodruff School of Mechanical Engineering, Georgia Institute of Technology, Atlanta, GA 30332, USA

^cSchool of Materials Science and Engineering, Georgia Institute of Technology, Atlanta, GA 30332, USA

Received 30 November 2011; received in revised form 5 March 2012; accepted 7 March 2012

Abstract

Stochastic, discontinuous flow is ubiquitous in the plastic deformation of small-volume metallic materials. We have identified a size-strengthening effect on the stress to initiate the jerky plastic yielding in nanoscale volumes of copper single crystals, subjected to nano-indentation in different orientations. Such a nanoscale size effect arises due to the stochastic nature of dislocation sources, in contrast to the microscale size effect often attributed to plastic strain gradients. The jerky response can result from the activation of either surface or bulk heterogeneous dislocation sources, as governed by the distribution and resistance of dislocation locks. Implications concerning the deformation mechanism in materials with flow defect-limited characteristics are discussed.

© 2012 Acta Materialia Inc. Published by Elsevier Ltd. All rights reserved.

Keywords: Nanoindentation; Yield phenomena; Dislocation; Molecular dynamics; Copper

1. Introduction

Plastic deformation in nanoscale volumes of materials often exhibits a stochastic, discontinuous character, in contrast to the typical smooth yield behavior in their bulk counterparts [1–7]. Such jerky behavior has been attributed to the instability of microscopic defect processes, such as dislocation nucleation or depinning in crystalline metals [8,9], phase transformation in semiconductors [10] and localized shear transformation in amorphous metals [11]. Despite recent intensive studies of jerky plastic deformation [12,13], its influence on macroscopic mechanical properties and the stochastic nature of the underlying defect processes are not well understood. A mechanistic understanding of those processes is essential to controlling the nanoscale deformation, which has implications for stabilizing nanostructures [14] and improving the reliability of micro/nanodevices [12,13].

In this paper, we present a coupled experimental and modeling study of the stochastic jerky plastic yielding, the so-called pop-in behavior, in single-crystal copper

(Cu) subjected to nanoindentation. We show that a size effect on yield strength arises due to the stochastic nature of dislocation sources in small volumes of crystals. Namely, the likelihood of activating a source of similar strength, which induces the dislocation avalanche and ensuing indenter displacement burst, decreases with the radius of the indenter tip and accordingly with the size of the highly stressed volume. This size-strengthening effect is fundamentally different from the microscale size effect often related to plastic strain gradients [15]. Furthermore, our results show that discontinuous yielding can be caused by the activation of either surface or bulk heterogeneous sources, with sensitivity to crystal orientations. Such features are expected to dominate the initiation of plastic flow in small-volume crystals with flow-defect-limited characteristics.

2. Methods

2.1. Theoretical analysis

During nanoindentation, the size of the highly stressed volume probed by the indenter tip is of the order of the contact diameter, typically in the range of a few to tens

* Corresponding author.

E-mail address: ting.zhu@me.gatech.edu (T. Zhu).

of nanometers. In such a small volume, the number of potential dislocation sources is severely limited and the yield events evolving from a single source become measurable, as manifested by displacement bursts in a load-controlled nanoindentation test [6]. The statistical distribution of source strengths can lead to the fluctuation of yield stresses for a fixed indenter size. More importantly, it can give rise to the size dependence of yield stress for measurements using different indenter sizes. Specifically, the stochastic nature of a single source can be characterized by using the weakest link concept and Weibull statistics [14,16]. It follows that the cumulative probability of discrete plastic yielding is given by [17]

$$f(\sigma, L) = 1 - \exp \left[- \left(\frac{L}{L_0} \right)^d \left(\frac{\sigma}{\sigma_0} \right)^m \right] \quad (1)$$

where L is the characteristic length scale of the highly stressed volume, σ is the average stress acting on this volume to represent an effective measure of applied (biasing) load that mechanically facilitates the activation of the dislocation source, d is the dimensionality of the source ($d=2$ for surface and $d=3$ for bulk defects), m is the Weibull modulus, L_0 is the reference length and σ_0 is the reference stress. Let us define the yield strength σ_Y as the critical stress that activates the source leading to dislocation avalanche and indenter displacement burst. The probability relation of Eq. (1) implies that σ_Y should satisfy the scaling law

$$\sigma_Y \propto L^{-\beta} \quad (2)$$

where the exponent $\beta = d/m$. For completeness, we derive Eq. (2) along the line of Rinaldi et al. [17]. Consider indentations by two different sized indenters. Denote the characteristic size of the highly stressed volume at the onset of indenter displacement burst as L and L_{ref} , respectively. A scaling law of yield strength is obtained by comparing two indentations at the same accumulative probability of discrete yielding, $f(\sigma_Y, L^d) = f(\sigma_{Yref}, L_{ref}^d)$, leading to $\sigma_Y/\sigma_{Yref} = (L_{ref}^d/L^d)^{1/m}$, which can be rewritten as Eq. (2).

According to Eq. (2), a statistical evaluation of d allows for the determination of whether surface ($d=2$) or volume ($d=3$) defects control the displacement bursts. Specifically, one can measure the yield strength from the initial bursts by using indenters of different radii R , and then fit the power law exponents β by taking the contact radius as the characteristic length scale L of the highly stressed volume. On the other hand, the Weibull modulus m can be evaluated by a statistical analysis of the variation in yield strengths, as will be detailed next. When both β and m are known, the dimensionality of the dislocation source d can be estimated according to $d = \beta m$. The value of d quantifies whether the operative sources are predominantly of surface or bulk character.

2.2. Nanoindentation experiment

Nanoindentation experiments were performed on Cu single crystals. These crystals (purity > 99.995%) were

grown by means of the Bridgman technique, and cut into a rectangular shape by spark erosion. The samples were mechanically polished to a surface roughness of $<0.05 \mu\text{m}$ by using grinding papers and diamond suspensions, and were then annealed in a vacuum chamber at 800°C for 6 h. After annealing, the samples were electropolished at room temperature using phosphoric acid/acetone/distilled water (1:1:2, v/v). The resultant surface roughness was $<3 \text{ nm}$, estimated by scanning probe microscopy.

The nanoindentation testing was performed by using a Hysitron triboindenter (Hysitron Inc., Minneapolis, MN, USA). Both a pyramid Berkovich tip (with a half included angle of 65.3°) and a cube-corner tip (with a half included angle of 42.28°) were used. The radii of the two tips were calibrated by indentations on a fused quartz and an Al(001) single crystal. The loads applied on the fused quartz were controlled below $50 \mu\text{N}$ to ensure elastic deformation. The rounded tip radius R was determined to be $164 \pm 10 \text{ nm}$ for the Berkovich tip and $53 \pm 4 \text{ nm}$ for the cube-corner tip.

Indentations were conducted normal to the (111), (110) and (100) surfaces under load control, with a constant loading rate \dot{P} between 10 and $500 \mu\text{N/s}$. We present in this paper the experimental data obtained at a low loading rate of $\dot{P} = 10 \mu\text{N/s}$, noting that the results are similar at higher loading rates. For each orientation, at least 300 indentations were measured for the statistical analysis of strength fluctuations, as facilitated by the high throughput of nanoindentation testing. The mean values of the reduced modulus for the (111) and (110) crystals are respectively 135 ± 10 and $138 \pm 8 \text{ GPa}$ – which are higher than that of the (100) crystal, $115 \pm 11 \text{ GPa}$ [18].

We determined the Weibull modulus, m , as follows. Eq. (1) can be recast into

$$\ln[\ln((1-f)^{-1})] = m \ln(\sigma/\sigma_0) + \ln[(L/L_0)^d] \quad (3)$$

so that

$$m = \frac{\partial \ln[\ln((1-f)^{-1})]}{\partial \ln \sigma} \quad (4)$$

Based on Eq. (4), the values of m were determined from the slope of the linear least-squares fitting curve for the accumulative probability f of displacement bursts as a function of the average stress σ acting on the highly stressed volume. Another often used measure of strength fluctuation is the activation volume Ω [19,20], which is related to the accumulative probability f by [21,22]

$$f = 1 - \exp \left(- \frac{\eta k T}{\dot{\sigma} \Omega} \exp \left(\frac{\sigma \Omega}{k T} \right) \right) \quad (5)$$

where k is the Boltzmann constant and T is the temperature; σ and $\dot{\sigma}$ are the applied stress and stress rate, respectively; and η is the nucleation rate in a stress-free crystal. From Eq. (5), Ω can be determined by

$$\Omega = k T \frac{\partial \ln[\ln((1-f)^{-1})]}{\partial \sigma} \quad (6)$$

Using Eqs. (4) and (6), one can readily show

$$m = \frac{\sigma\Omega}{kT} \quad (7)$$

Here we emphasize that the Weibull modulus m is a more general measure of strength fluctuation than the activation volume Ω . The latter primarily characterizes the temperature and strain-rate effects on strength variation. In contrast, the former further captures the effects of the distribution of source strengths. Moreover, the Weibull statistical relation of Eq. (1) is the basis for revealing the size effect caused by the extreme value statistics of dislocation sources in the dislocation-starved deformation regime.

2.3. Nanoindentation modeling

Using the interatomic potential finite element method (IPFEM) [23–25], we have studied the nanoindentation-induced homogeneous dislocation nucleation in a dislocation-free perfect crystal of Cu as a possible cause of experimentally measured displacement bursts. The IPFEM simulation was performed based on the formulation and numerical procedure developed in our previous works [23–25]. The key ingredient of the IPFEM is the interatomic potential-based constitutive relation derived within the framework of hyperelasticity (i.e. nonlinear elasticity) with the Cauchy–Born rule. As such, the IPFEM allows us to capture the homogeneous dislocation nucleation resulting from the lattice instability caused by elastic softening at large strains. The interatomic interaction is modeled by an embedded atom method potential of Cu [26], which was validated by comparing with experimental results and ab initio calculations. We implemented the IPFEM in the finite element package ABAQUS/Explicit by writing user material subroutines.

Using the IPFEM, we have performed three-dimensional simulations of nanoindentation by a spherical indenter. The critical states of homogeneous dislocation nucleation were quantitatively characterized. Predictions were given as to when and where the dislocation would nucleate, and what slip mode the nucleated dislocation would take. More specifically, nanoindentation was simulated for a spherical indenter pressed into the (111), (110) and (100) surfaces of single-crystal Cu, respectively. The radius of the indenter was 50 nm, corresponding to the approximate tip size of the nominally sharp indenter used in experiments. The spherical indenter was modeled as a frictionless, analytic rigid surface. The system has an in-plane size of 300×300 nm and a depth of 600 nm. The boundary conditions were imposed as follows: the displacement along the bottom of the mesh is constrained to be zero, while the displacements of lateral surfaces are unconstrained. The graded mesh comprises eight-node linear brick elements, with a typical element size of about 10 Å near the indenter. The total number of elements was 519,332. The indenter was moved down under displacement control at a sufficiently low rate to mimic the quasi-static loading condition, as calibrated by the

analytic solutions for indentation on a linear anisotropic elastic material [24].

Homogeneous dislocation nucleation in a perfect crystal can be triggered by the nonlinear elastic instability of crystal lattice at large strains. The onset of instability is associated with the Hadamard condition of loss of positive definiteness of the matrix Q_{jk} , defined by $Q_{jk} = n_i(c_{ijkl} + \sigma_{jk}\delta_{ij})n_l$, for any unit vector n_i [24]. Here, the current and reference configurations of the crystal lattice are assumed to coincide; σ_{jk} is the Cauchy (true) stress and c_{ijkl} is the tangent (instantaneous elastic) modulus, both of which are calculated from the interatomic potential. For small deformation, Q_{jk} is positive definite. When $\det(Q_{jk}) = 0$, a loss of stability occurs, leading to dislocation nucleation. Correspondingly, the unit vector n_i predicts the activated slip plane, and the eigenvector associated with the matrix Q_{jk} predicts the slip direction at the onset of dislocation formation.

Molecular dynamics (MD) simulations were also performed to directly reveal the dislocation nucleation and post-nucleation behavior. Owing to the time scale limitation of MD, simulations were conducted for a small system, i.e. a cube ($\sim 100,000$ atoms) with an approximate side length of 10 nm. The indentation loading rate was high (~ 6 m s⁻¹). A spherical indenter with a radius of 5 nm was pressed into the (111), (110) and (100) surfaces, respectively. The location and atomic structure of embryonic dislocation loops from MD simulations were consistent with predictions from IPFEM simulations, as discussed next.

3. Results and discussion

Fig. 1a and c shows the representative load–displacement (P – h) curves from indentation by a Berkovich tip and a cube-corner tip, respectively. The displacement burst has a length of about 2–10 nm, corresponding to approximately 8–40 slip events of dislocation annihilation at the surface, each of which leads to a surface offset on the order of the Burgers vector magnitude ($b = 0.256$ nm for Cu). Fig. 1b and d shows the corresponding frequency histograms of P_c and h_c at the onset of displacement bursts. Table 1 presents their mean and standard deviation for each indentation orientation. From these data we estimate the critical contact radius $a_c \approx \sqrt{R h_c}$ based on the Hertzian solution of elastic contact [27]. Here we ignore the influence of dislocation activities on the contact geometry, as it is expected to be limited prior to the indenter displacement burst. On this basis, the yield stress, σ_Y , acting on the highly stressed volume can be approximated by using P_c divided by the contact area at the moment of displacement bursts. The values of σ_Y and a_c are used as the measures of stress and length in Eq. (2), respectively.

The indentation size effects on yield strength are revealed in Fig. 2. It can be seen that the cube-corner indenter ($R \approx 50$ nm) gives a small a_c and a large σ_Y , considerably different from the results measured using the Berkovich indenter ($R \approx 160$ nm). By fitting to the power-law

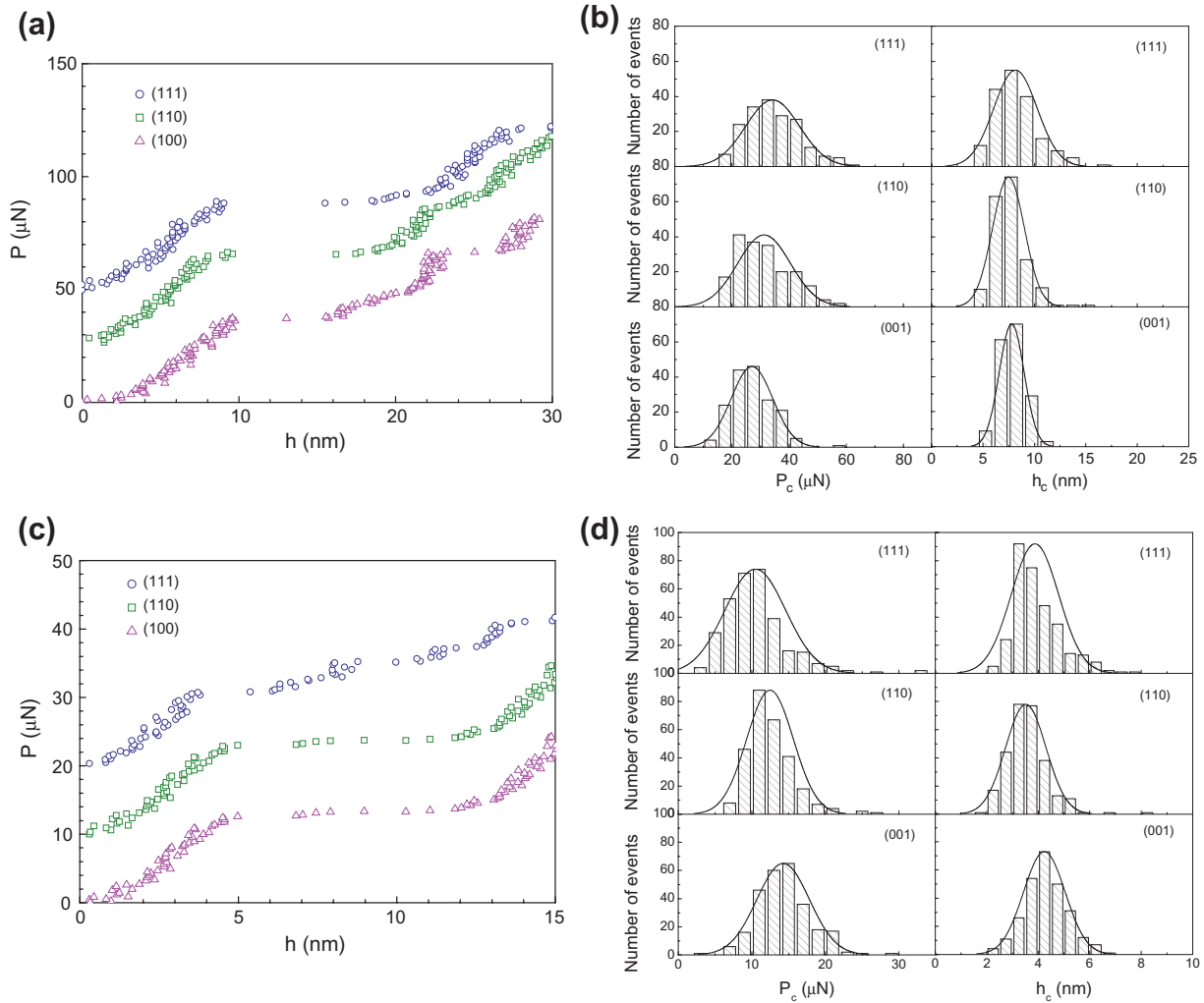


Fig. 1. Experimental results of nanoindentation on the (111), (110) and (100) surfaces of single-crystal Cu. (a) Representative load–displacement curves and (b) frequency histograms of the critical indenter force P_c and displacement h_c at the onset of displacement bursts for the Berkovich tip (tip radius $R = 164 \pm 10$ nm). In (a) the origin of the indenter force P is shifted for the (111) and (110) cases, and in (b) each nanoindentation orientation includes about 300 indents. (c) Same as (a), and (d) same as (b), except for the cube-corner tip (tip radius $R = 53 \pm 4$ nm).

Table 1

The indenter force P_c and displacement h_c at the onset of initial displacement bursts from nanoindentation experiments, together with the power-law exponent β , the Weibull modulus m and the dimensionality of dislocation source $d = \beta m$.

Indentation plane	Berkovich tip ($R = 164$ nm)		Cube-corner tip ($R = 53$ nm)		β	m	d
	P_c (μN)	h_c (nm)	P_c (μN)	h_c (nm)			
(111)	34.2 ± 9.4	8.2 ± 2.1	10.5 ± 4.1	3.9 ± 0.9	0.22	8.11	1.8
(110)	31.2 ± 9.2	7.4 ± 1.5	12.5 ± 3.2	3.5 ± 0.8	0.27	7.49	2.0
(100)	27.0 ± 7.3	7.8 ± 1.2	14.3 ± 3.6	4.2 ± 0.8	0.49	5.67	2.8

relation of Eq. (2), the exponent β is determined as given in Table 1. Here the nanoindentation size effect arises in concert with extreme value statistics of dislocation sources. Namely, the likelihood of activating a dislocation source of similar strength, which induces the dislocation avalanche and ensuing indenter displacement burst, decreases as the radius of the indenter tip (i.e. the size of the highly stressed volume) decreases. As a result, a higher load is needed to

initiate the process. This size effect contrasts with that of microindentation [15,28], which has been attributed to plastic strain gradients originating from the injection of a number of geometrically necessary dislocations configured to achieve compatible deformation beneath the micron-sized indenter. The physics in this case differs entirely from that of our nanoindentation experiments, as they do not involve a dislocation source limited behavior. In addition,

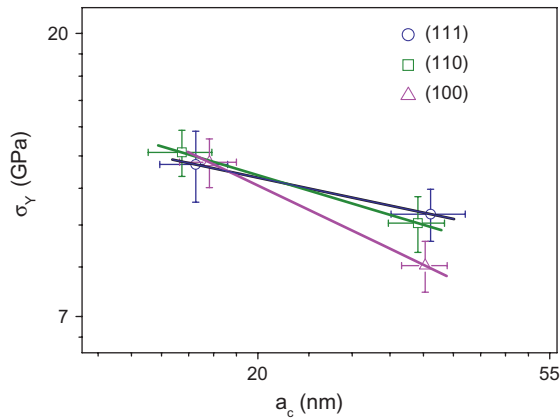


Fig. 2. Double logarithmic plot of yield stress σ_Y (defined as the indenter force over the contact area at the onset of the displacement burst) vs. corresponding indenter contact radius a_c . The left cluster pertains to the cube-corner tip, while the right cluster is associated with the Berkovich tip.

Gerberich et al. [29] have studied the nanoindentation size effect arising from the indentation depth dependence of surface and volume work. They attributed the plastic work to the motion of a number of dislocations, which also fundamentally differs from the dislocation-starved regime considered here.

According to Eq. (1), the fluctuation of yield strengths in nanoindentation can be characterized by using the Weibull modulus. The lower the Weibull modulus m , the higher the variability of yield strength, which corresponds to a wider probability distribution and a larger scatter of data. Table 1 lists the values of m obtained using the statistical procedure as described in Section 2.2. Here we emphasize that the Weibull modulus is a more general measure of strength fluctuation than the often used activation volume [21], as discussed in Section 2.2. In particular, the measured Weibull modulus m and the power-law exponent β allow us to determine the dimensionality of dislocation sources $d = \beta m$, as given in Table 1. These results indicate that bulk defects ($d \approx 3$) are most likely responsible for the displacement bursts in the case of (100) indentation. In contrast, surface defects ($d \approx 2$) are most likely underlying the bursts in the (111) and (110) indentations.

As in Ref. [17], the above Weibull analysis is conducted to characterize the statistical nature of a major regenerative dislocation source that can lead to the experimentally measurable jerky response due to the source activation and ensuing dislocation avalanche. However, it should be noted that, unlike Ref. [17], which studied nanopillars subjected to uniform compression, the stress field is non-uniform beneath a nanoindenter. As a first approximation, we take the average stress in the highly stressed volume under the nanoindenter to represent an effective measure of the applied (biasing) load, which mechanically facilitates the activation of the dislocation source. The probability of such an activation process can be affected by the non-uniformity of the stress distribution. However, in the spirit of Weibull statistics, the influence of the non-uniform local

stress is not explicitly considered, but is embedded into the Weibull modulus instead. Mason et al. [30] studied such a kind of uniform stress approximation in detail. In their work, the activation volume was used to characterize the statistical temperature and strain-rate effects on source activation; note that the activation volume can be related to the Weibull modulus by Eq. (7). Their results (the first two rows in Table 1 [30]) show that the activation volumes estimated from the “first-order model” with a constant stress approximation are close to those from the “second-order model”, which captures the full complexity of the non-uniform stress field beneath a nanoindentation. This provides direct support to the validity of using the average stress as an effective measure of applied loads.

The dependence of operative dislocation sources on the crystallographic orientation of indentation is unexpected, and its origin is not yet fully understood. Recent in situ nanoindentation experiments in a transmission electron microscope enable the observation of dislocation nucleation and propagation [31]. However, a direct correlation has not been established between the nature of the dislocation sources and the displacement bursts. Moreover, while there is a large body of literature on the modeling of incipient plasticity during nanoindentation [6], the physical processes underlying the major discontinuous yielding events have not been elucidated. Motivated by the experiments, we investigated the indentation orientation effects on dislocation nucleation by using both the IPFEM and MD simulations along the same line of our previous works [23–25]; a brief summary of the principles and numerical procedures has been given in Section 2.3.

Using the IPFEM, we study the nanoindentation-induced homogeneous dislocation nucleation in a dislocation-free perfect crystal as a possible cause of experimentally measured displacement bursts. As noted in Section 2.3, the IPFEM enables nanoindentation simulations at the experimental size scale while retaining the atomic-scale resolution. We consider the homogeneous dislocation nucleation resulting from the hyperelastic (non-linear elastic) instability [24]. When the indenter radius R is 50 nm, the critical indenter displacements for nucleation are predicted as $h_c^{(111)} : h_c^{(110)} : h_c^{(100)} = 5.04 \text{ nm} : 3.85 \text{ nm} : 1.93 \text{ nm} \approx 2.6 : 2 : 1$, with the corresponding nucleation sites shown in Fig. 3a. These ratios have been verified qualitatively by direct MD simulations in smaller systems ($R = 5 \text{ nm}$), as shown in Fig. 3b; and they can also be rationalized by evaluating the Schmid factors or resolved shear stresses on the most favorably oriented slip systems for nucleation [25]. Importantly, while these predictions are within the range of experimental values of h_c (as given in Table 1), they disagree qualitatively with the measured ratios that exhibited a considerably weak orientation dependence. Such differences provide quantitative evidence that discontinuous yielding should be triggered by the activation of heterogeneous sources, rather than the homogeneous dislocation nucleation in a small volume of perfect crystal beneath the indenter tip.

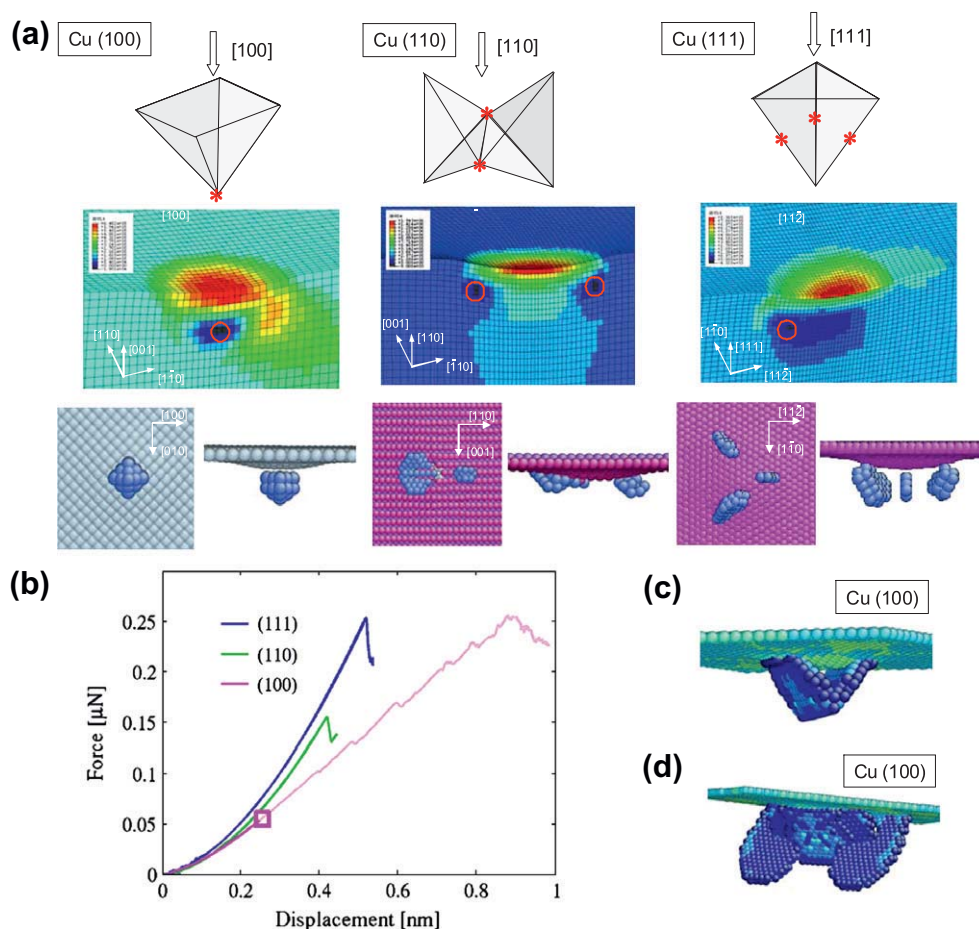


Fig. 3. Modeling of nanoindentation on the (111), (110) and (100) surfaces of single-crystal Cu. (a) Dislocation nucleation sites. Upper: schematics (stars); middle: IPFEM predictions (circles) when the indenter radius $R = 50$ nm; lower: MD simulations when $R = 5$ nm. Atoms are colored by the coordination number and the perfectly coordinated atoms are removed to show the surface and dislocation embryos. (b) Indenter load–displacement responses from MD simulations. (c) Post-nucleation dislocation structures for the (100) indentation at a small indentation penetration. (d) Same as (c) except at a large indenter displacement. In both (c) and (d), atoms are colored by the central symmetry parameter to show the wedge-shape lock junction bounded by two stacking faults on the $\{111\}$ slip planes. (For interpretation of the references to color in this figure legend, the reader is referred to the web version of this article.)

In order to understand the effect of crystallographic orientation on the dislocation sources responsible for the indenter displacement bursts in experiments, we performed direct MD simulations to study the post-homogeneous nucleation behavior in nanoindentation. Our MD simulation was performed in a displacement-controlled mode, such that the discontinuous yielding event is shown as a load drop rather than a displacement burst under force control. Fig. 3b shows that, in the (100) indentation, the load drop is not observed immediately after the initial homogeneous nucleation event (as indicated by the square symbol); the indenter force continues to increase, and a significant load drop occurs at a much larger force, as also reported by Liang et al. [32]. Such a hardening response arises because of the immediate formation of dislocation locks. In particular, the nucleation site and the site of lock formation coincide, both being located at the central axis where the four equivalent slip systems (indicated by shaded triangles) intersect (see Fig. 3a). Note that the lock junction creates a wedged-shape region bounded by the two $\{111\}$ slip

planes (see Fig. 3c), which restricts the plastic deformation inside the wedge and prevents a significant load drop. Moreover, the wedge transmits the indenter load and generates a stress concentration at its tip. At larger indenter penetrations, the load drops occur due to the heterogeneous dislocation nucleation from the junctions near the wedge tip (see e.g. Fig. 3d). Considering the dominant effect of bulk dislocation junctions on stress relaxation in the (100) indentation, we propose that such a type of dislocation lock can act as a heterogeneous source to initiate dislocation avalanches, which in turn lead to the experimentally measured indenter displacement burst. This source is located inside the crystal, consistent with the Weibull analysis of the (100) nanoindentation experiment ($d \approx 3$).

In contrast, MD simulations show that, for both the (111) and (110) indentations, the load drops occur immediately after the first nucleation event. In particular, no major locks form owing to the fact that several equivalent nucleation sites are located off the central axis and at different locations, as shown in Fig. 3a. This facilitates the

escape of dislocations to the surface, as well as injection into the bulk. The former process creates the heterogeneous surface sources that could initiate dislocation avalanches, leading to the indenter displacement burst. In these two cases, the locations of heterogeneous sources are consistent with those from the Weibull analysis of experiments ($d \approx 2$).

We note that it is possible that there are already dislocation activities before the first jerky jump, as shown in the in situ nanoindentation experiments inside a transmission electron microscope of Minor et al. [31]. However, such minor dislocation activities are not manifested as the significant pop-in that can give the measured displacement jump in the typical range of 2–10 nm, which corresponds to 8–40 slip processes of dislocation annihilation at the surface. As such, they are not the object of our Weibull statistical analysis. Here the Weibull statistics are used to characterize the activation of the strong regenerative dislocation source that can lead to an experimentally measurable, significant jerky response. Furthermore, we note that, while MD simulations are limited to the very early stage of nanoindentation responses, the results reveal an important effect of (100) orientation on the easy formation of dislocation locks. Further crystallography analysis (Fig. 3a) shows that this effect is governed by the converging geometry of slip planes, which is unique to the (100) nanoindentation and should be insensitive to the loading rate of MD. On this basis, we propose that the nanoindentation-induced dislocation lock might physically correspond to the heterogeneous bulk source, as inferred from the measured dimensionality of the dislocation source ($d \approx 3$) for (100) nanoindentation. Since the present MD simulations are focused on the orientation effect, systematic MD studies are needed in the future to directly explore the statistical aspects of strength fluctuation and size effects.

4. Conclusions

We have studied stochastic, discontinuous plastic deformation in nanoscale volumes of single-crystal Cu. In contrast to the microscale size effect, often attributed to plastic strain gradients and geometrically necessary dislocations, a fundamentally different mechanism of size strengthening is shown to arise in concert with the stochastic nature of dislocation sources. The results also demonstrate that the crystallography of plastic shear can significantly influence the activation of stochastic plastic deformation in materials with flow defect-limited characteristics. Our work integrates the statistical theory, high-throughput nanoindentation testing, and atomistic and coarse-grained IPFEM modeling, to provide an effective paradigm to study the deformation mechanism at the nanoscale. Finally, we note that, while extreme care has been taken to minimize the surface roughness (<3 nm) in sample preparation, the influence of imperfect surfaces cannot be completely excluded during the indentation testing [33,34]. The experimental results on the nucleation

statistics, however, are expected to be robust, as the analysis was based on hundreds of nanoindentations. Nevertheless, further experimental and modeling studies are needed to better understand the role of pre-existing surface defects (e.g. steps and oxide films) on size effects and strength fluctuation at the nanoscale.

Acknowledgements

W.W. is supported by the NSF of China (Grant 50571097). K.L. and L.L. are supported by the NSF of China (Grants 50621091, 50431010, 50725103, and 50890171) and the Ministry of Science and Technology of China (Grant 2005CB623604). D.L.M. and T.Z. are supported by the NSF (Grant CMMI-0758265). L.L. and T.Z. are supported by the CAS/SAFEA international partnership program for Creative Research Team. We thank Professor W.D. Nix for critical comments on the paper.

References

- [1] Greer JR, Nix WD. *Phys Rev B* 2006;73:245410.
- [2] Volkert CA, Lilleodden ET. *Philos Mag* 2006;86:5567.
- [3] Ng KS, Ngan AHW. *Philos Mag* 2008;88:677.
- [4] Gerberich WW, Nelson JC, Lilleodden ET, Anderson P, Wyrobek JT. *Acta Mater* 1996;44:3585.
- [5] Kiely JD, Houston JE. *Phys Rev B* 1998;57:12588.
- [6] Gouldstone A, Chollacoop N, Dao M, Li J, Minor AM, Shen YL. *Acta Mater* 2007;55:4015.
- [7] Shim S, Bei H, George EP, Pharr GM. *Scripta Mater* 2008;59:1095.
- [8] Li J, Van Vliet KJ, Zhu T, Yip S, Suresh S. *Nature* 2002;418:307.
- [9] Dimiduk DM, Woodward C, LeSar R, Uchic MD. *Science* 2006;312:1188.
- [10] Jang JI, Lance MJ, Wen SQ, Tsui TY, Pharr GM. *Acta Mater* 2005;53:1759.
- [11] Schuh CA, Hufnagel TC, Ramamurty U. *Acta Mater* 2007;55:4067.
- [12] Zhu T, Li J. *Prog Mater Sci* 2010;55:710.
- [13] Greer JR, De Hosson JTM. *Prog Mater Sci* 2011;56:654.
- [14] McDowell DL. *Mater Sci Eng R – Rep* 2008;62:67.
- [15] Nix WD, Gao HJ. *J Mech Phys Solids* 1998;46:411.
- [16] Sieradzki K, Rinaldi A, Friesen C, Peralta P. *Acta Mater* 2006;54:4533.
- [17] Rinaldi A, Peralta P, Friesen C, Sieradzki K. *Acta Mater* 2008;56:511.
- [18] Wang W, Lu K. *Philos Mag* 2006;86:5309.
- [19] Zhu T, Li J, Samanta A, Leach A, Gall K. *Phys Rev Lett* 2008;100:025502.
- [20] Jennings AT, Li J, Greer JR. *Acta Mater* 2011;59:5627.
- [21] Schuh CA, Mason JK, Lund AC. *Nat Mater* 2005;4:617.
- [22] Schuh CA, Lund AC. *J Mater Res* 2004;19:2152.
- [23] Van Vliet KJ, Li J, Zhu T, Yip S, Suresh S. *Phys Rev B* 2003;67:104105.
- [24] Zhu T, Li J, Van Vliet KJ, Ogata S, Yip S, Suresh S. *J Mech Phys Solids* 2004;52:691.
- [25] Zhong Y, Zhu T. *Comput Methods Appl Mech Eng* 2008;197:3174.
- [26] Mishin Y, Farkas D, Mehl MJ, Papaconstantopoulos DA. *Phys Rev B* 1999;59:3393.
- [27] Johnson KL. *Contact mechanics*. Cambridge: Cambridge University Press; 1985.
- [28] Swadener JG, George EP, Pharr GM. *J Mech Phys Solids* 2002;50:681.
- [29] Gerberich WW, Tymiak NI, Grunlan JC, Horstemeyer MF, Baskes MI. *J Appl Mech* 2002;69:433.
- [30] Mason JK, Lund AC, Schuh CA. *Phys Rev B* 2006;73:054102.

- [31] Minor AM, Asif SAS, Shan ZW, Stach EA, Cyrankowski E, Wyrobek TJ, Warren OL. *Nat Mater* 2006;5:697.
- [32] Liang HY, Woo CH, Huang HC, Ngan AHW, Yu TX. *CMES – Comput Model Eng Sci* 2004;6:105.
- [33] Zimmerman JA, Kelchner CL, Klein PA, Hamilton JC, Foiles SM. *Phys Rev Lett* 2001;87:165507.
- [34] Navarro V, de la Fuente OR, Mascaraque A, Rojo JM. *Phys Rev Lett* 2008;100:105504.